ADVANCED MATERIALS INTERFACES
Open Access
www.advmatinterfaces.de

Probing the Interfacial Molecular Structure of a Co-Prussian Blue In Situ

Anupam Bera, Ratnadip De, Heiner Schmidt, Desirée Leistenschneider, Turkan Gamze Ulusoy Ghobadi, Martin Oschatz, Ferdi Karadaş, and Benjamin Dietzek-Ivanšić**

Molecular-level insight into the interfacial composition of electrodes at the solid-electrolyte and the solid-electrode interface is essential to understanding the charge transfer processes, which are vital for electrochemical (EC) and photoelectrochemical (PEC) applications. However, spectroscopic access to both interfaces, particularly upon application of an external bias, remains a challenge. Here, in situ surface sensitive vibrational sum-frequency generation (VSFG) spectroscopy is used for the first time to directly access the interfacial structure of a cobalt-containing Prussian blue analog (Co-PBA) in contact with the electrolyte and TiO_2/Au surface. Structural and compositional changes of the Prussian blue layer during electrochemical oxidation are studied by monitoring the stretching vibration of the CN group. At open circuit potential, VSFG reveals a non-homogeneous distribution of oxidation states of metal sites: Fe^{III}–CN–Co^{II} and Fe^{II}–CN–Co^{III} coordination motifs are dominantly observed at the Co-PBA|TiO_2 interface, while it is only the Fe^{II}–CN–Co^{II} unit at the electrolyte interface. Upon increasing the potential applied to the electrode, the partial oxidation of Fe^{II}–CN–Co^{II} to Fe^{III}–CN–Co^{II} is observed followed by its transformation to Fe^{II}–CN–Co^{III} via charge transfer and, finally, the formation of Fe^{III}–CN–Co^{III} species at the interface with TiO_2 and the electrolyte.

1. Introduction

Solid-solid and solid-liquid interfaces, serving as the conduits for charge, energy, and information transfer, play determining roles in a range of technological applications, e.g., photovoltaic devices, secondary-ion batteries, solar cells, and electrochemical (EC), photocatalytic (PC), and photoelectrochemical (PEC) applications.[1] Understanding interfaces has become crucial to define the efficiency of these underlying processes, which rely heavily on their ability to separate and transfer charge within distinct components efficiently. While ex situ techniques have furnished valuable insights, they often fall short of capturing the dynamic nature of real operating conditions. Consequently, techniques that enable the in situ exploration of interface dynamics, chemical reactions, and charge transport mechanisms have been developed to bridge the gap between fundamental understanding and practical applications of interfaces.[2]

Cobalt-containing Prussian blue analogs (Co-PBAs) represented with the general molecular formula $(K_xCo^a[Fe^b(CN)_6]_y.zH_2O$, where a, b are formal oxidation states, and x, y, and z are stoichiometric coefficients) are acknowledged as robust, effective, and inexpensive electrodes for sodium/potassium-ion batteries and electrocatalytic processes including water, glucose, and alcohol oxidation processes.[3] Furthermore, Co-PBA has

A. Bera, R. De, H. Schmidt, F. Karadaş, B. Dietzek-Ivanšić
Department of Functional Interfaces
Leibniz Institute of Photonic Technology Jena
Albert-Einstein-Strasse 9, 07745 Jena, Germany
E-mail: karadas@fen.bilkent.edu.tr; benjamin.dietzek@leibniz-ipht.de
A. Bera, R. De, H. Schmidt, F. Karadaş, B. Dietzek-Ivanšić
Institute of Physical Chemistry
Friedrich Schiller University Jena
Helmholtzweg 4, 07743 Jena, Germany
The ORCID identification number(s) for the author(s) of this article can be found under https://doi.org/10.1002/admi.202400009

DOI: 10.1002/admi.202400009

D. Leistenschneider, M. Oschatz
Institute of Technical and Environmental Chemistry Jena
Friedrich Schiller University Jena
Philosophenweg 7a, 07743 Jena, Germany
D. Leistenschneider, M. Oschatz, B. Dietzek-Ivanšić
Center for Energy and Environmental Chemistry Jena
Philosophenweg 7a, 07743 Jena, Germany
T. G. Ulusoy Ghobadi
NANOTAM – Nanotechnology Research Center
Bilkent University
Ankara 06800, Turkey
M. Oschatz
Helmholtz Institute for Polymers in Energy Applications Jena
(HIPOLE Jena)
Lessingstraße 12–14, 07743 Jena, Germany

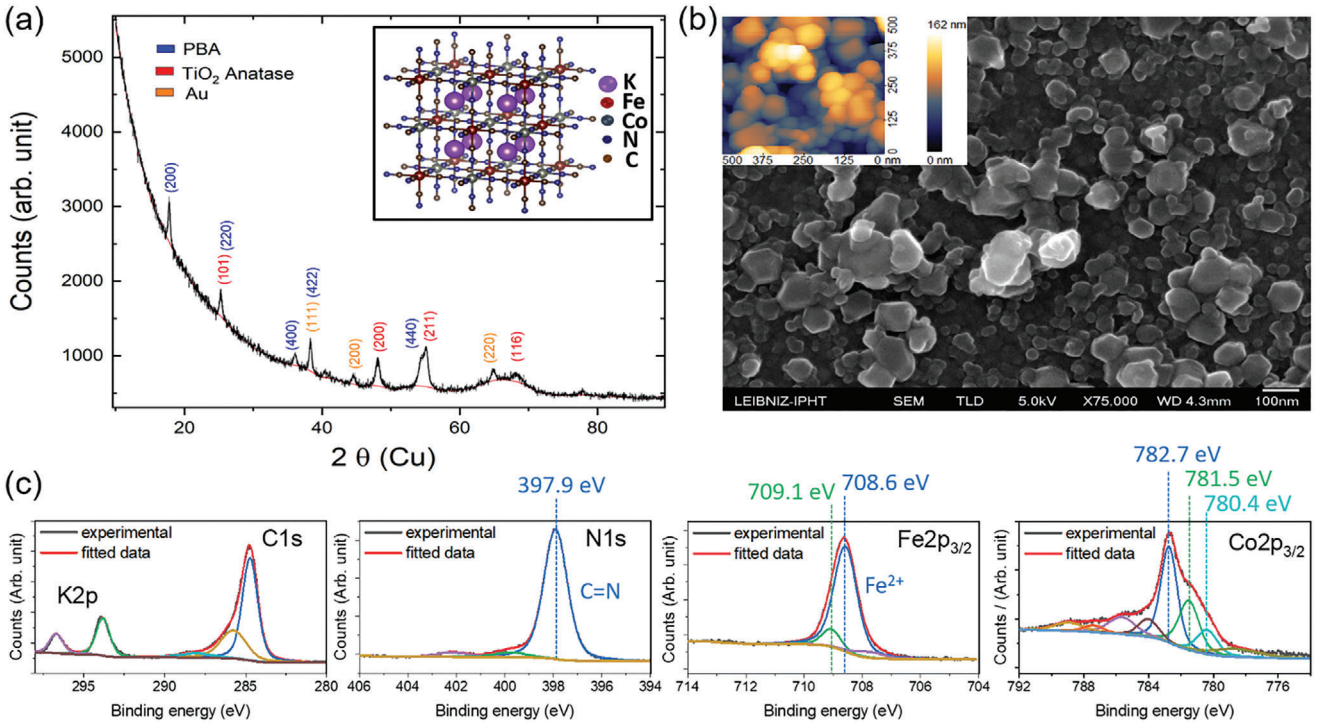

Figure 1. a) Schematic representation of the molecular structure of the Co-PBA and grazing incidence X-ray Diffraction (GIXRD) pattern, b) SEM images (the inset shows AFM images), and c) respective C 1s with K 2p, N 1s Fe 2p, and Co 2p XPS spectra.

been used to modify semiconductor electrodes, such as TiO_2, $BiVO_4$, and Fe_2O_3, and following this strategy electrodes have been developed for PC and PEC water oxidation and organic pollutant degradation processes.[4] The structure of Co-PBA consists of metal ions connected through cyanide bridging ligands to form a 3D extended network (see **Figure 1**a inset).[3a] The Fe–CN–Co coordination motif affords intrinsic charge transfer between metal ions, which plays a key role in the catalytic process. In electrocatalytic processes both Co and Fe sites exist in two oxidation states, i.e., 2+ and 3+, to yield a mixed-valent compound, which is sensitive to the type of solid and liquid interfaces. Although operando techniques have been used to elucidate the charge transfer process within the bulk PB structure and from the PB layer to the semiconductor, they are unable to distinguish the bulk of the material from the interface.[4e,5] Therefore, an interface-selective technique is needed to understand the charge transfer processes in Prussian blue-derived mixed-valent compounds. In this context, we utilize vibrational sum-frequency generation (VSFG) spectroscopy, a unique and powerful surface-specific tool,[6] which has been applied to study interfaces for EC and PEC applications.[2a,7] However, in general, VSFG is a 2nd order nonlinear process, and the overall signal compared to the IR techniques is very low. Nevertheless, accessing buried interfaces with VSFG spectroscopy between liquid-solid or solid-solid remains challenging due to their strong IR absorption and low overall VSFG signal. To overcome this, earlier studies often used a cell with a thin layer of electrolytic solution between the electrode and the cell window.[7e,g,8] However, it results in severe mass transport limitations and diffusion-controlled kinetics. The second method is for the visible and infrared beams to approach the interface through the electrode known as the internal reflection method.[9] However, it requires the use of a transparent electrode or films with an average thickness of less than 10 nm which often unstable and cannot sustain the current densities. In our case, the VSFG intensity is recorded in a conventional reflection way with an electrolyte layer thickness of ≈250 μm. The overall VSFG enhancement happened due to the presence of a strong nonresonant background originating from the TiO_2/Au substrate. Furthermore, the selected $TBABF_4$/DCM electrolyte solvent pair exhibits very low IR absorption in the —CN vibrational regions. Additionally, a homogeneous and uniform Co-PBA has been designed to improve the signal-to-noise ratio.

Herein, we present the first in situ VSFG probing of the structural and compositional changes in the interfaces of a Co-PBA thin film deposited on a TiO_2/Au substrate during an EC oxidation process. Our methodology begins by evaluating the primary constituents at the surface and subsurface interfaces using VSFG spectroscopy and X-ray photoelectron spectroscopy (XPS) prior to characterizing the EC oxidation process. Since the VSFG technique is inherently a probe of broken centrosymmetry, the VSFG

F. Karadaş
Department of Chemistry
Main Campus
Bilkent University
Ankara 06800, Turkey
F. Karadaş
UNAM – National Nanotechnology Research Center
Bilkent University
Ankara 06800, Turkey

data characterizes the composition of a single layer of the Prussian blue analog film at the interface in direct contact with the liquid electrolyte and electrode surface. In addition, potentialdependent in situ VSFG data provide insight into the oxidation states of metal sites and their respective compositions.

2. Results and Discussion

While a variety of methods, including spin coating, electrodeposition, and insitu synthesis, have been used to prepare Co-PBA-modified electrodes, we developed a new technique to fabricate a uniform Prussian blue layer on TiO_2 in order to improve the signal-to-noise ratio in the VSFG experiments.[10] The TiO_2/Au substrates were allowed to stay in a heated solution of Co-PBA, which afforded a film thickness of ≈90 nm (see Figure S1, Supporting Information). The film possesses a cubic lattice structure with metal atoms connected by bridging CN groups, as shown in Figure 1a. Figure 1b illustrates the morphology of the Co-PBA structure, displaying sizes distributed from 17 to 114 nm in the SEM image and accompanying AFM image. Prior to the in situ VSFG experiments, an ex situ XPS study was performed to determine the elemental ratio and oxidation state of Co and Fe in the surface layer. The element analysis suggests a Co/Fe ratio of 0.9:1 ± 0.1 and the K-content in the surface layer is ≈2.6 at.% (see Table S1 and Figure S2, Supporting Information). The layer composition is estimated to be $K_{0.5}Fe_1Co_{0.9}(CN)_{4.2}$. In addition, the HR XPS spectra of C, N, $Fe2p_{3/2}$, and $Co2p_{3/2}$ are depicted in Figure 1c. XPS reveals the presence of C 1s peaks at 284.8, 285.7, and 287.0 eV. Binding energies for C in cyanide ligands such as in Prussian blue, are reported to be in a range between ≈284 and ≈286 eV for the respective hexacyano complexes.[11] The N1s spectrum is also analyzed as contributions from adventitious carbon at ≈284.7 eV cannot be excluded. The N1s spectrum shows peaks at three distinct binding energies, i.e., 397.9, 400.0, and 402.3 eV, which are assigned to the different bonding environments of nitrogen in C≡N, N–H, and $N_{oxides,}$ which is in good agreement with the Prussian blue structure.[11] Additionally, a visible peak of $Fe2p_{3/2}$ at 708.6 eV represents only Fe^{II} species. The presence of Fe^{III}, which would show as a peak at binding energy around ≈710 eV, cannot be identified in the $Fe2p_{3/2}$ spectrum.[12] The peak present around ≈709.1 eV could possibly originate from Fe^{II} bonded through the N in cyanide instead of a Fe^{II}–C-bonding motif as N is the more electronegative bonding partner.[12] Additionally, the $Co2p_{3/2}$ spectrum indicates the presence of 2+ as an oxidation state. However, a clear assignment of Co^{II} and Co^{III} is difficult due to the multiple splitting, the contribution of the satellite peaks, and the broadness of the peaks.[13] However, for the Co2p spectrum, the peak with the highest intensity is found at 782.7 eV. A binding energy of ≈780.4 eV points to a Co^{II} component while the one at 782.7 eV could be attributed to Co^{III}, but also originate from multiplet splitting of the Co^{II}.[11] While the synthesis of the Co-PBA (using $Co(NO_3)_2$•$6H_2O$ as a precursor) should yield Co^{II} species exclusively, partial oxidation to Co^{III} in the pristine film, which is possibly created during the synthesis at high temperatures. Moreover, the ratio of Co/Fe, which is calculated from the XPS data varies slightly within the layer, which could additionally affect the Co2p signal and shift the binding energies due to different chemical environments.[14] Therefore, it is difficult to derive a final conclusion about the oxidation states for Co using XPS. It is also important to note that XPS analysis doesn't directly relate to the interface composition. In comparison, as discussed in the next section, VSFG is utilized to characterize Co-PBA present at the Co-PBA|TiO_2 and Co-PBA|electrolyte interfaces.

Figure 2a,b illustrate the experimental setup for in situ VSFG experiments and the VSFG spectra of ≈90 nm Co-PBA thin film deposited on TiO_2/Au, respectively. The spectrum was recorded at open circuit potential (OCP) in ppp polarization combinations (polarization of SF, visible, and IR respectively) in 2000–2230 cm^{-1} region to probe the CN stretching vibrations with VSFG. The assignment of oxidation states of metal ions based on the CN stretching wavenumbers is a well-established method in cyanide chemistry.[5] As shown in Figure 2b, VSFG measurement reveals three distinct bands in the interface, corresponding to Fe^{II}–CN–Co^{II}, Fe^{II}–CN–Co^{III}-A, and Fe^{III}–CN–Co^{II} units, at 2105, 2119, and 2160 cm^{-1}, respectively. It should be noted that the Fe^{II}–CN–Co^{III} composition gives rise to two characteristic bands at ≈2120 and ≈2137 cm^{-1}, depending on the relative K^+ ion concentration, which are referred to as type -A and -B throughout the manuscript.[5b] The signal at 2119 cm^{-1} in the VSFG spectrum (see Figure 2b) reveals the presence of the Fe^{II}–CN–Co^{III}-A coordination motif, suggesting the presence of a high K^+ ion concentration. Moreover, we calculated the respective resonant contributions from fitting the VSFG spectrum, yielding information about the relative population of each band (grey line in Figure 2b). The vertical sticks indicate the strength of each band. These intensities represent an approximate measure of the relative contribution of Fe^a–CN–Co^b units to the overall VSFG signal. We estimate Fe^{II}–CN–Co^{II}, Fe^{II}–CN–Co^{III}-A, and Fe^{III}–CN–Co^{II} to contribute to the signal by about 54%, 25%, and 21%, respectively. The exact peak position, width, and corresponding oscillator strengths utilized for the line strength calculation are displayed in Table S2 (Supporting Information). Additionally, the red line in Figure 2b shows the ATR-FTIR spectrum of the same Co-PBA film. The ATR-FTIR single peak at 2135 cm^{-1} represents the Fe^{II}–CN–Co^{III}-B coordination motif. Since the ATR-FTIR probing depth is in the range between 100 nm and several μm, it cannot be considered a surface-sensitive technique.[15] On the other hand, VSFG is a second-order nonlinear technique that provides interface-sensitive and selective molecular information where symmetry is broken, which explains the absence of Fe^{II}–CN–Co^{III}-B units, representing the bulk compositions of Co-PBA. Nevertheless, a combined analysis of ATR-FTIR and VSFG spectra provides complete 3D structural information of the bulk structures and interfaces.

Furthermore, the appearance of the VSFG spectrum in Figure 2b is notably different than regular FTIR spectra. More specifically, the VSFG spectrum shows a dispersive line shape instead of a regular Lorentzian profile and exhibits peaks for Fe^{II}–CN–Co^{II}, Fe^{II}–CN–Co^{III}-A, and a dip for Fe^{III}–CN–Co^{II} units. These characteristics are common in VSFG measurements of molecules adsorbed onto metallic/metal oxide interfaces and indicate a different orientation of the oscillating dipole at the surface.[16] In our results, the resonant part, which contains –CN vibrations of the –Fe–CN–Co units, interferes with the nonresonant background from the TiO_2/Au surface. The spectral fit shown in Figure 2b indicates a relative phase of 2.6 ± 0.2 (i.e.,150°± 10°) between the peak and dip. As we will argue

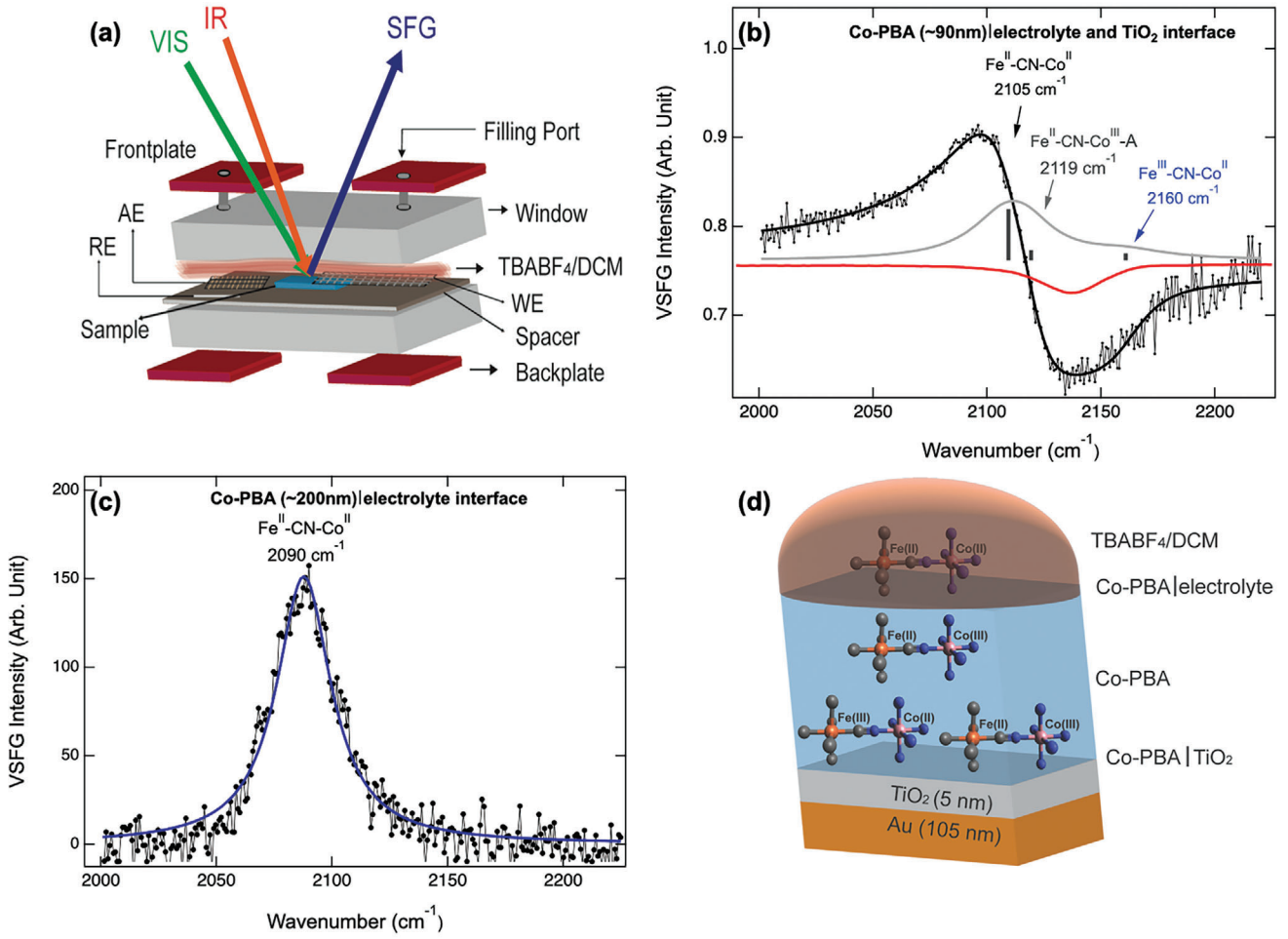

Figure 2. a) Schematic illustration of the electrochemical cell for in situ VSFG measurements. b) ppp VSFG spectrum (polarization of SF, visible, and IR, respectively) of a Co-PBA film deposited on TiO_2/Au substrate before applying potential in 1 mM $TBABF_4$/DCM solution. This spectrum is influenced by the non-resonant background stemming from the TiO_2/Au film. The black solid line represents the fit to the data. The grey solid line is the linear ppp spectrum calculated using the parameters obtained from the fit and offset by the level of the non-resonant background. The three bands as contributing are identified. The vertical sticks indicate the strength of each band. The inset red solid line is the FTIR spectra recorded from the same sample. c) ppp VSFG spectra of the more than twofold thicker (≈200 nm) Co-PBA film deposited on TiO_2/Au substrate recorded at open circuit potential in 1 mM $TBABF_4$/DCM solution. This spectrum has a Lorentzian line shape as there is no influence of the background non-resonant signal. d) The schematic diagram of the interfaces and respective Co-PBA composition present at Co-PBA|TiO_2-and electrolyte and the Co-PBA|electrolyte interface.

below, the ability of VSFG to probe both interfaces of the Co-PBA film, i.e., the Co-PBA|electrolyte and the Co-PBA|TiO_2 interface, can additionally contribute to the observed phase difference and spectral shape.

We also investigated a significantly thicker Co-PBA film (thickness of ≈200 nm) to gain insight into the contributions of the TiO_2|Co-PBA and the Co-PBA|electrolyte interfaces to the observed VSFG signal. Studying the thick Co-PBA film, we eliminate the interference between the non-resonant background stemming from the TiO_2/Au layer with the vibrationally resonant signal from the Co-PBA|electrolyte interface.[17] Figure 2c shows the resultant VSFG spectrum of the thick Co-PBA. The spectrum reflects a single Lorentzian band stemming from Fe^{II}–CN–Co^{II} units. This feature is solely present at the electrolyte interface (depicted in Figure 2d). The observed red shift of the band compared to the thin Co-PBA layer is due to the presence of more K^+ ions, which is suggested by angle-resolved XPS (Figure S4, Supporting Information). The latter experiment indicates an increased K^+ concentration towards the surface (see Figure S4, Supporting Information). Furthermore, the VSFG finding also suggests that the other two compositions (reported in Figure 2b), i.e., Fe^{II}–CN–Co^{III}-A and Fe^{III}–CN–Co^{II}, are formed at the Co-PBA|TiO_2 interface. Figure 2d depicts all compositions present at different interfaces at the Co-PBA film. As indicated above, the phase difference or the presence of peaks and dips between Fe^{II}–CN–Co^{II} and Fe^{III}–CN–Co^{II} can be explained by contributions of the two distinct Co-PBA interfaces to the overall VSFG signal.

The Co-PBA|TiO_2/Au substrate has been scrutinized thus far under open circuit potential conditions. In the next step, we will investigate the Co-PBA|TiO_2/Au sample in situ, i.e., upon applying an electrical potential, to elucidate the impact of electrochemical oxidation of the various metal centers in PBA on the vibrational characteristics of the cyano-bridges. **Figure** 3a shows the cyclic voltammetric (CV) profile of the

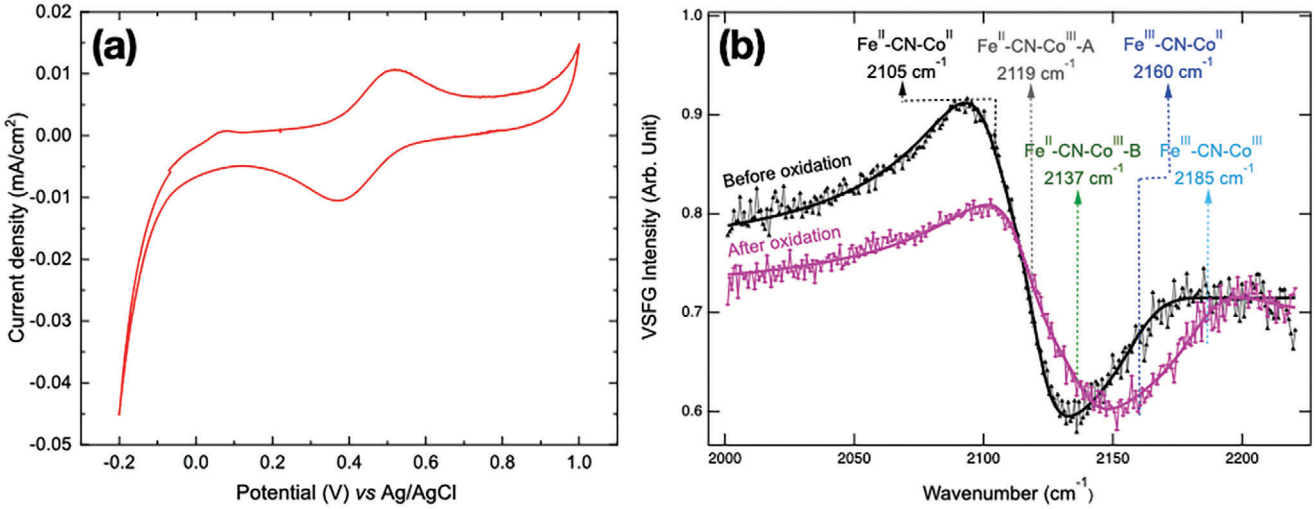

Figure 3. a) The CV of Co-PBA|TiO_2/Au electrode in 1 mM TBABF_4/DCM solution in the −0.2–+1.0 V (vs Ag/AgCl) potential range. b) Comparative VSFG spectra of the electrode before and after the redox process were recorded at −0.1 (black color spectrum) and 0.9 V (magenta color spectrum) versus Ag/AgCl, respectively. The compositions before oxidation are Fe^{II}–CN–Co^{II}, Fe^{II}–CN–Co^{III}-A, and Fe^{III}–CN–Co^{II} as also observed at OCP (Figure 2b) while the compositions after oxidation are Fe^{II}–CN–Co^{III}-A, Fe^{II}–CN–Co^{III}-B, and Fe^{III}–CN–Co^{III}.

Co-PBA|TiO_2/Au electrode in 1 mM TBABF_4/Dichloromethane (DCM) solution in the −0.2–+1.0 V (vs Ag/AgCl) potential range. An oxidation process is observed at 0.5 V versus the Ag-AgCl reference electrode. The width of the peak is attributed to the presence of two overlapping oxidation processes, i.e., Fe^{II}→ Fe^{III} and Co^{II}→ Co^{III}.[18] Additionally, a small irreversible redox peak at 0.06 V is observed, which originates from the bare TiO_2/Au surface. The CV of the bare TiO_2/Au has been plotted in the supporting information (Figure S6, Supporting Information). This small local peak is often attributed to the charge transfer between intraband gap localized states, which originates due to partially coordinated surface Ti atoms.[19]

In situ VSFG spectra upon oxidation of Co-PBA|TiO_2/Au electrode were recorded in a chronoamperometric fashion at different potentials (see **Figure** 4a). Figure 3b shows VSFG spectra of the first structural characteristics before and after the oxidation process. The spectra, recorded for Co-PBA|TiO_2/Au, are fitted with the function given in Equation S1 (see Experimental Methods in Supporting Information). From the fitting, we determine the normalized oscillator strength of the i-th component (A_i), which presents a measure of the concentration of the individual Fe^a-CN-Co^b units (see Equation S2, Supporting Information). Figure 4b presents an analysis of the distribution of oxidation states upon variation of the potential.

2.1. In Situ VSFG in the Potential Range Between Open Circuit Potential and 0.7 V (Anodic Scan)

At open circuit potential (OCP), three coordination motifs are discernible based on the VSFG spectra: Fe^{II}–CN–Co^{II}, Fe^{II}–CN–Co^{III}-A, and Fe^{III}–CN–Co^{II} (vide supra in the context of Figure 2). No spectral changes are observed upon increasing the potential to 0.1 V, i.e., remaining below the onset of the electrochemical oxidation feature. At potentials more positive than OCP, the Fe^{II}–CN–Co^{II} unit, decreases in intensity, while the Fe^{III}–CN–Co^{II} unit, increases. The first major spectral change occurs at 0.2 V as the Fe^{III}–CN–Co^{II} unit signal increases 1.75 times in comparison to the OCP state. We attribute this potential-dependent signal increase to the partial Fe^{II} → Fe^{III} oxidation to yield Fe^{III}–CN–Co^{II} units. Moreover, at 0.7 V, the Fe^{III}–CN–Co^{II} unit signal reached its maximum intensity (increased by 2.6 times), while Fe^{II}–CN–Co^{II} decreased by a factor of 1.4 compared to the OCP. Furthermore, a slight, ca. 10%, increase is observed in the Fe^{II}-CN-Co^{III}-A unit, indicating that the onset of Co^{II} → Co^{III} oxidation process is reached. This is consistent with the broad oxidation peak observed in CV at 0.5 V in the anodic scan (Figure 3a) It is important to note that a small vibrational redshift of 2–4 cm^{-1} is observed in the CN vibration before 0.7 V, and up to 7 cm^{-1} at higher potentials from 0.7 V. This is most likely due to the vibrational Stark effect as previously reported for CN group which is a well-known Stark reporters.[20]

2.2. In Situ VSFG at Potentials More Positive than 0.7 V (Anodic Scan)

At voltages more positive than 0.7 V versus Ag/AgCl, significant spectral changes become visible; i.e., the peaks associated with the Fe^{II}–CN–Co^{II} and Fe^{III}–CN–Co^{II} units at 2105 and 2160 cm^{-1}, respectively, vanish. Concertedly, two new peaks emerge at 2137 and 2185 cm^{-1}, attributed to Fe^{II}–CN–Co^{III}-B and Fe^{III}–CN–Co^{III} units, respectively. The profile suggests that, at anodic potentials more positive than 0.7 V, the Fe^{II}–CN–Co^{II} and Fe^{II}–CN–Co^{III} units are oxidized yielding Fe^{II}–CN–Co^{III} and Fe^{III}–CN–Co^{III}, respectively. In addition, Fe^{II}–CN–Co^{III}-A also attains its highest intensity. A potential increase from 0.9 to 1.2 V does not lead to further spectroscopic changes, indicating that the composition of oxidation states remains constant in this potential window. It should be pointed out that the spectral changes are reversible, i.e., a cathodic scan of potentials from positive potentials to OCP can

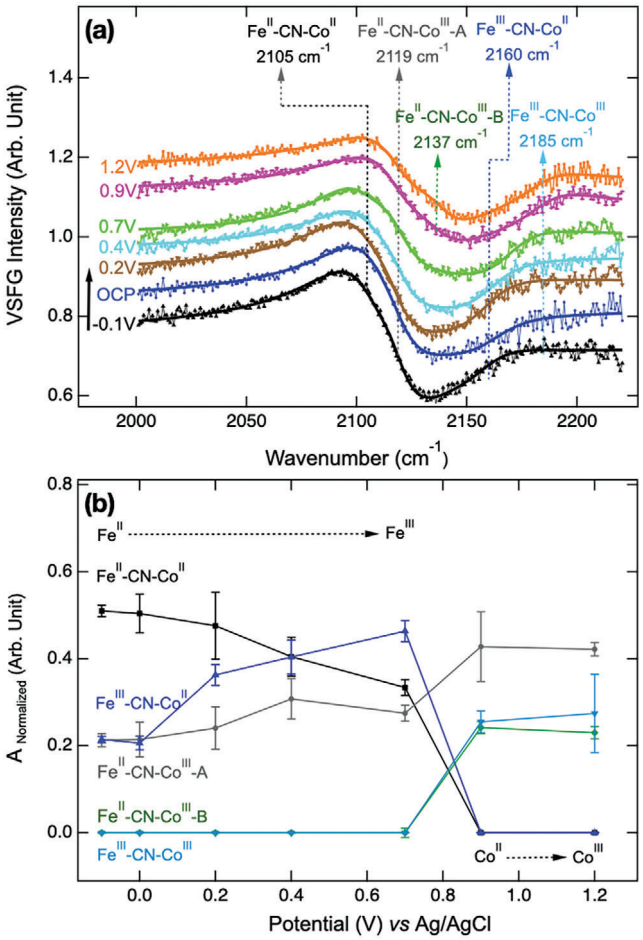

Figure 4. a) An in situ VSFG spectra of a Co-PBA film deposited on TiO_2/Au substrate in 1 mM $TBABF_4$/DCM solution at stepwise increasing potentials (−0.1, 0, 0.2, 0.4, 0.7, 0.9, and 1.2 V). The spectra represent the CN stretching vibration of Fe^a-CN-Co^b units. The curves were vertically offset to ease visual inspection of the data. b) Oscillator strength (A_i) of the individual species of the deconvoluted VSFG bands as a function of potential from the spectra in Figure 3a. The A_i is proportional to the relative contribution of a species to the overall signal. The spectra were normalized versus OCP data.

reproduce the results discussed above (see Figure S7, Supporting Information). In this potential scan, all structural formation is related to the oxidation of the cobalt center ($Co^{II} \rightarrow Co^{III}$). Therefore, the VSFG not only correlates with the main voltammetric processes observed by the CV but also provides significant information about the interfacial structure of Co-PBA, which is crucial for understanding charge transfer mechanisms for EC and PEC applications.

3. Conclusion

In summary, surface-specific in situ VSFG spectroscopy elucidated the compositional and electronic evolution of Co-PBA interfaces during the electrochemical oxidation of the material. The methodology is applied for the first time to Prussian Blue analogs and reveals structural and oxidation-state information from both the Co-PBA|electrolyte and the Co-PBA|TiO_2-electrode interfaces. Our findings showcase that the metal sites in the interface undergo different structural changes than the ones in the bulk. The advancement of surface and interface-sensitive techniques is critical to distinguish potentially catalytically active sites from the bulk of the material and to unravel the catalytic mechanism. The happy pairing of VSFG and electrochemistry provides us with the platform to investigate the photocatalytic and photochemical properties of Prussian blue structures at suitable interfaces. Our molecular-level analysis of the electrolyte-electrode interface provides the basis for a variety of scientific and technological applications, including energy storage and electrocatalysis.

Supporting Information

Supporting Information is available from the Wiley Online Library or from the author.

Acknowledgements

The authors thank Dr. Keshav Kumar Jha and Wolfgang Paa for their help in designing the VSFG setup, Jan Dellith, Marco Diegel for their support with AFM and XRD measurements, Uwe Hübner and Mario Ziegler for their support with the thin film fabrication. The authors appreciate many helpful discussions with the Hasselbrink-group (University of Duisburg-Essen) for the optimization of the VSFG set up. The work was financially supported by the Carl-Zeiss-Foundation via the *Durchbrüche-Programm* (project *Intelligente Substrate: Schaltbare Grenzflächen auf Basis multiresponsiver Hybridmaterialien*). B.D.I. acknowledge support by the German Science Foundation (INST 275/402-1). F.K. would like to acknowledge the Humboldt foundation for George Forster Research Award from the Alexander von Humboldt Foundation 2022. M.O. and B.D.I. further acknowledge financial support within the Research Unit ThüNaBsE – Thuringian Sodium Battery from for Scalable Energy Storage (FTI Thüringen PERSONEN, 2023 FGR 0066),supported by the Free State of Thuringia and the European Social Fund Plus. D.L would like to thank the German Chemical Industry Fund for the financial support through a Leibig Fellowship.

Open access funding enabled and organized by Projekt DEAL.

Conflict of Interest

The authors declare no conflict of interest.

Data Availability Statement

The data that support the findings of this study are available from the corresponding author upon reasonable request.

Keywords

charge transfer process, electrode-electrolyte interface probe, in situ vibrational sum-frequency generation, Prussian blue analogues, spectroelectrochemistry

Received: January 5, 2024
Revised: March 27, 2024
Published online: April 29, 2024

[1] a) S. Shao, M. A. Loi, *Adv. Mater. Interfaces.* **2020**, *7*, 1901469; b) A. Chandra, G. Anderson, S. Melkote, W. Gao, H. Haitjema, K. Wegener,

CIRP Ann. **2014**, *63*, 797; c) J. Popovic, *Nat. Commun.* **2021**, *12*, 6240; d) P. F. van Hutten, G. Hadziioannou, *The role of interfaces in photovoltaic devices*, Springer, Berlin, Heidelberg **2001**.

[2] a) R. De, B. Dietzek-Ivanšić, *Chemistry.* **2022**, *28*, 202200407; b) L. Meyer, N. Saqib, J. Porter, *J. Electrochem. Soc.* **2021**, *168*, 090561.

[3] a) K. Itaya, I. Uchida, V. D. Neff, *Acc. Chem. Res.* **1986**, *19*, 162; b) L. Wang, J. Song, R. Qiao, L. A. Wray, M. A. Hossain, Y.-D. Chuang, W. Yang, Y. Lu, D. Evans, J.-J. Lee, *J. Am. Chem. Soc.* **2015**, *137*, 2548; c) Q. Wang, J. Li, H. Jin, S. Xin, H. Gao, *InfoMat.* **2022**, *4*, 12311; d) T. Matsuda, Y. Moritomo, *Appl. Phys. Express.* **2011**, *4*, 047101; e) Q. Liu, Z. Hu, M. Chen, C. Zou, H. Jin, S. Wang, S. L. Chou, Y. Liu, S. X. Dou, *Adv. Funct. Mater.* **2020**, *30*, 1909530.

[4] a) T. G. Ulusoy Ghobadi, E. Ozbay, F. Karadas, *Chemistry.* **2021**, *27*, 3638; b) M. Xu, K. Li, S. Wang, S. Zhou, H. Zhang, H. Xu, J. Zhao, Y. Li, *Nano Res.* **2023**, *16*, 3294; c) L. Feng, N. Li, S. Tang, Y. Guo, J. Zheng, X. Li, *Inorg. Chem. Commun.* **2021**, *125*, 108349; d) C. Shi, S. Ye, X. Wang, F. Meng, J. Liu, T. Yang, W. Zhang, J. Wei, N. Ta, G. Q. Lu, *Adv. Sci.* **2021**, *8*, 2001987; e) B. Moss, F. S. Hegner, S. Corby, S. Selim, L. Francas, N. r. López, S. Gimenez, J.-R. N. Galán-Mascarós, J. R. Durrant, *ACS Energy Lett.* **2018**, *4*, 337.

[5] a) H. Niwa, T. Moriya, T. Shibata, Y. Fukuzumi, Y. Moritomo, *Sci. Rep.* **2021**, *11*, 4119; b) R. O. Lezna, R. Romagnoli, N. R. De Tacconi, K. Rajeshwar, *J. Phys. Chem. B.* **2002**, *106*, 3612.

[6] Y. Shen, *Proc. Natl. Acad. Sci.* **1996**, *93*, 12104.

[7] a) M. A. Hines, J. Todd, P. Guyot-Sionnest, *Langmuir.* **1995**, *11*, 493; b) A. Tadjeddine, A. Peremans, *J. Electroanal. Chem.* **1996**, *409*, 115; c) H. Noguchi, T. Okada, K. Uosaki, *Faraday Discuss.* **2009**, *140*, 125; d) J. Lahann, S. Mitragotri, T.-N. Tran, H. Kaido, J. Sundaram, I. S. Choi, S. Hoffer, G. A. Somorjai, R. Langer, *Science.* **2003**, *299*, 371; e) S. Rivera-Rubero, S. Baldelli, *J. Phys. Chem. B.* **2004**, *108*, 15133; f) G. Zwaschka, F. Lapointe, R. K. Campen, Y. Tong, *Curr. Opin. Electrochem.* **2021**, *29*, 100813; g) R. L. Behrens, A. Lagutchev, D. D. Dlott, A. Wieckowski, *J. Electroanal. Chem.* **2010**, *649*, 32.

[8] a) W.-T. Liu, Y. R. Shen, *Proc. Natl. Acad. Sci.* **2014**, *111*, 1293; b) Y. Tong, F. Lapointe, M. Thämer, M. Wolf, R. K. Campen, *Angew. Chem., Int. Ed.* **2017**, *56*, 4211.

[9] a) J. Löbau, K. Wolfrum, *J Opt Soc Am B.* **1997**, *14*, 2505; b) N. Nishi, D. Hobara, M. Yamamoto, T. Kakiuchi, *Anal. Sci.* **2003**, *19*, 887; c) G. Tourillon, L. Dreesen, C. Volcke, Y. Sartenaer, P. A. Thiry, A. Peremans, *Nanotechnology.* **2007**, *18*, 415301.

[10] a) E. P. Alsaç, E. Ülker, S. V. K. Nune, Y. Dede, F. Karadas, *Chemistry.* **2018**, *24*, 4856; b) S. Pintado, S. Goberna-Ferrón, E. C. Escudero-Adán, J. R. Galán-Mascarós, *J. Am. Chem. Soc.* **2013**, *135*, 13270; c) E. Usman, M. Barzgar Vishlaghi, S. Sadigh Akbari, F. Karadas, S. Kaya, *ACS Appl. Energy Mater.* **2022**, *5*, 15434; d) M. Aksoy, S. V. K. Nune, F. Karadas, *Inorg. Chem.* **2016**, *55*, 4301; e) A. A. Karyakin, *Electroanalysis.* **2001**, *13*, 813.

[11] N. Vannerberg, The Esca-Spectra of Sodium and Potassium Cyanide and of The Sodium and Potassium Salts of The Hexacyano-Metallates of The First Transition Metal Series **1976**. https://dx.doi.org/10.18434/T4T88K

[12] a) A. Grosvenor, B. Kobe, M. C. Biesinger, N. McIntyre, *Surf. Interface Anal.* **2004**, *36*, 1564; b) P. Somani, A. Mandale, S. Radhakrishnan, *Acta Mater.* **2000**, *48*, 2859.

[13] D. Briggs, V. Gibson, *Chem. Phys. Lett.* **1974**, *25*, 493.

[14] T. Chuang, C. Brundle, D. Rice, *Surf. Sci.* **1976**, *59*, 413.

[15] N. Harrick, *Phys. Rev. Lett.* **1960**, *4*, 224.

[16] T. Balgar, H. Kim, E. Hasselbrink, *J. Phys. Chem. Lett.* **2013**, *4*, 2094.

[17] a) Z. Chen, Y. Shen, G. A. Somorjai, *Annu. Rev. Phys. Chem.* **2002**, *53*, 437; b) J. Wang, Z. Paszti, M. A. Even, Z. Chen, *J. Phys. Chem. B.* **2004**, *108*, 3625.

[18] D. Ellis, M. Eckhoff, V. Neff, *J. Phys. Chem.* **1981**, *85*, 1225.

[19] a) F. Fabregat-Santiago, I. Mora-Seró, G. Garcia-Belmonte, J. Bisquert, *J. Phys. Chem. B.* **2003**, *107*, 758; b) G. Redmond, D. Fitzmaurice, M. Graetzel, *J. Phys. Chem.* **1993**, *97*, 6951.

[20] D. Wright, S. Sangtarash, N. S. Mueller, Q. Lin, H. Sadeghi, J. J. Baumberg, *J. Phys. Chem. Lett.* **2022**, *13*, 4905.